Inorganic Chemistry

Article

pubs.acs.org/IC

Isomer-Directed Structural Diversity and Its Effect on the Nanosheet Exfoliation and Magnetic Properties of 2,3-Dimethylsuccinate Hybrid Frameworks

Paul J. Saines,[†] Mark Steinmann,[†] Jin-Chong Tan,[†,‡] Hamish H.-M. Yeung,[†] Wei Li,[†] Phillip T. Barton,[§,∥] and Anthony K. Cheetham*[,†]

[†]Department of Materials Science and Metallurgy, The University of Cambridge, Cambridge CB2 3QZ, United Kingdom

[‡]Department of Engineering Science, University of Oxford, Parks Road, Oxford OX1 3PJ, United Kingdom

[§]Materials Department, University of California, Santa Barbara, California 93106, United States

[∥]Materials Research Laboratory, University of California, Santa Barbara, California 93106, United States

Supporting Information

ABSTRACT: The structures of seven new transition metal frameworks featuring Mn, Co, or Zn and either the *meso* or chiral D and L isomers of the 2,3-dimethylsuccinate ligand are reported. Frameworks that exhibit two-dimensional covalently bonded layers with weak interlayer interactions can be made with all three cations by incorporation of the chiral isomers of the 2,3-dimethylsuccinate ligand. The formation of such structures, suitable for the creation of nanosheets *via* exfoliation, is, however, not as ubiquitous as is the case with the 2,2-dimethylsuccinate frameworks since frameworks that incorporate the *meso*-2,3-dimethylsuccinate ligand form three-dimensional structures. This clear distinction between the formation of structures with covalent connectivity in two and three dimensions, depending on the choice of 2,3-dimethylsuccinate isomer, is due to the different conformations adopted by the backbone of the ligand. The chiral isomer prefers to adopt an arrangement with its methyl and carboxylate groups *gauche* to the neighboring functional groups of the same type, while the *meso*-ligand prefers to adopt *trans* geometry. A *gauche*-arrangement of the methyl groups places them on the same side of the ligand, making this geometry ideal for the formation of layered structures; a *trans*-relationship leads to the methyl groups being further apart, reducing their steric hindrance and making it easier to accommodate them within a three-dimensional structure. The ease of exfoliation of the layered frameworks is examined and compared to those of known transition metal 2,2-dimethylsuccinate frameworks by means of UV−vis spectroscopy. It is suggested that layered frameworks with more corrugated surfaces exfoliate more rapidly. The size, structure, and morphology of the exfoliated nanosheets are also characterized. The magnetic properties of the paramagnetic frameworks reveal that only the three dimensionally covalently bonded phases containing *meso*-2,3-DMS in *trans*-arrangements order magnetically. These frameworks are antiferromagnets at low temperatures, although the Co compound undergoes an unusual antiferromagnetic to ferromagnetic transition with increasing applied magnetic field.

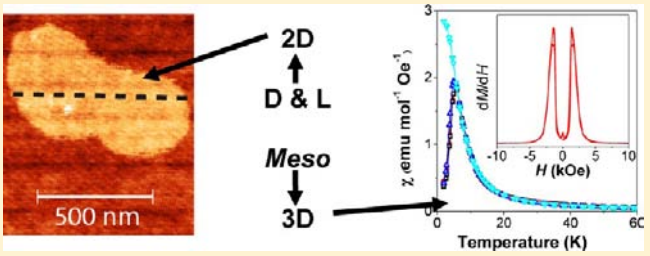

1. INTRODUCTION

Hybrid inorganic−organic framework materials have attracted significant interest over the past decade due to the fascinating range of structures and wide variety of useful properties these compounds exhibit.[1−5] The structures of these hybrid materials are influenced significantly by both their cation and ligand building blocks, and they can adopt either porous or dense structures. Porous frameworks, often referred to as metal−organic frameworks (MOFs), are of significant interest due to their catalytic, gas storage, and separation properties,[3,4,6,7] while dense frameworks attract interest for their ability to exhibit cooperative behavior more commonly associated with purely inorganic materials, such as magnetic order, semiconductivity, and multiferrocity.[8−10] While the majority of studies of hybrid frameworks have focused on the synthesis of single crystals and powders with micrometer-sized particles, significant attention has recently been drawn to the possibility of making nanosized particles of these materials, to allow them to be incorporated into thin films for technological applications.[11−15] Such studies have usually focused on exploring the various "bottom-up" approaches by which these materials could be synthesized, and the subsequent investigation of how the properties of these nanoparticles differ from the bulk phase. It has, however, been recently shown that crystallites of frameworks featuring covalently bound 2D layers with weak interlayer interactions

Received: September 15, 2012
Published: October 2, 2012

   dx.doi.org/10.1021/ic302011x | Inorg. Chem. 2012, 51, 11198−11209

can be exfoliated by ultrasonication into nanosheets with lateral sizes of the order of micrometers and thicknesses of only tens of nanometers.[16−19] This "top-down" approach is cost-effective and readily achieved, as shown by a number of recent examples among a wider range of materials,[20−22] and is likely to be particularly useful in the case of dense frameworks as they lack the guest molecules found in the cavities of porous structures, which potentially complicate the exfoliation process.

While producing nanosheets *via* ultrasonication-induced exfoliation appears promising, the preparation of framework nanosheets requires a hybrid material with a suitable layered structure in its bulk phase. Among the dense frameworks, we have recently shown that a number of layered structures suitable for nanosheet exfoliation featuring different cations and topologies can be prepared using the 2,2-dimethysuccinate ligand (2,2-DMS), $(CO_2C(CH_3)_2CH_2CO_2)^{2-}$.[18,19] These structures have covalent connectivity in two dimensions but only interact in the third through weak van der Waals forces, which allows their layers to be easily separated through ultrasonication. We have suggested that the topology of a material can have a significant effect on the relative dimensions of the nanosheets produced. It is therefore important to produce materials with a wide range of cations and topologies to better understand what factors affect the ease of exfoliation and the size and topologies of the nanosheets that result from this.[19] 2,2-DMS belongs to a larger family of succinate-related ligands that lack the bulky aromatic groups of their more rigid relatives. They have attracted significant attention due to the large variety of framework structures into which they can be incorporated, leading to some of these compounds exhibiting highly unusual magnetic behavior.[23−31] None of the other flexible dicarboxylates, however, have been shown to consistently produce layered structures capable of being readily exfoliated into nanosheets.

This work investigates the possibility of using the 2,3-dimethylsuccinate (2,3-DMS) ligand, $(CO_2CH(CH_3)CH(CH_3)CO_2)^{2-}$, from sources containing either a mixture of D-, L-, and *meso*-isomers or the pure *meso*-form in combination with transition metal cations, namely Mn^{2+}, Co^{2+}, and Zn^{2+}, to make layered frameworks suitable for exfoliation. The methyl groups are further apart in 2,3-DMS than in the 2,2-isomer, and this may have an effect on the exfoliation process. It could, however, also lead to frameworks exhibiting other ways of accommodating the bulky methyl groups in their structures. Furthermore, this may, in part, depend on the orientation adopted by the backbone of the ligand and its effect on the relative positions of the substituent groups. This study reports seven new 2,3-DMS transition metal frameworks and finds that layered frameworks suitable for exfoliation can be made with all three cations. It is, however, shown that such layered structures are not as ubiquitous as in the case of those structures incorporating 2,2-DMS. Specifically, a clear distinction was found between the structures adopted by ligands incorporating the chiral and *meso*-isomers of the 2,3-DMS ligand. The topology and morphologies of the nanosheets formed for the three layered phases are characterized, and their ease of exfoliation is examined and compared to those of selected 2,2-DMS transition metal frameworks. The magnetic properties of the Mn^{2+} and Co^{2+} frameworks examined in this study are also studied, with several of the three-dimensional phases found to order magnetically.

2. EXPERIMENTAL SECTION

All seven compounds reported in this work were made using commercially available starting materials, *via* 3 day hydrothermal synthesis in 23 mL Teflon-lined Paar autoclaves at temperature equal to or below 200 °C. Details of the stoichiometry and overall connectivity of each framework, the metal and ligand from which they were synthesized, and the temperature range over which they form are presented in Table 1. Further details of the synthetic conditions used to prepare single crystals and pure bulk samples are presented in the ESI alongside details of the experimental procedure used for structure determinations. Crystallographic details and cation−oxygen bond distances are shown in Tables 2 and S1, respectively.

Table 1. Reaction Conditions Used To Form Each Structure Examined in This Study and the Stoichiometry and Connectivity of the Resulting Framework[a]

structure	metal and ligand used	reaction temp (°C)	final product	connectivity[32]
1	Mn, mixed-2,3-DMS	90−125	$Mn_3(DL)_3(H_2O)_2$	2D (I^1O^1)
2	Mn, mixed-2,3-DMS	150−200	Mn(*meso*)	3D (I^2O^1)
2	Mn, *meso*-2,3-DMS	180−200	Mn(*meso*)	3D (I^2O^1)
3	Mn, *meso*-2,3-DMS	125−200	Mn(*meso*)	3D (I^1O^2)
4	Mn, *meso*-2,3-DMS	100	Mn(*meso*) $(H_2O)\cdot H_2O$	3D (I^1O^2)
5	Co, mixed-2,3-DMS	90−200	Co(DL)(H_2O)	2D (I^1O^1)
6	Co, *meso*-2,3-DMS	180−200	Co(*meso*)	3D (I^1O^2)
7	Zn, mixed-2,3-DMS	70−200	Zn(DL)	2D (I^0O^2)
7	Zn, *meso*-2,3-DMS	150−200	Zn(DL)	2D (I^0O^2)

[a] Mixed-2,3-DMS refers to a mixture of D-, L- and *meso* dimethylsuccinic acid, while in the final product DL and *meso* refer to structures containing a 1:1 mixture of D- and L-isomers and *meso*-2,3-DMS, respectively.

Powder X-ray diffraction (PXRD) patterns of all samples were collected using Cu Kα radiation on a Bruker D8 Advance diffractometer equipped with a position sensitive linear detector. Results from this indicated that compounds **2**−**4** and **7** were obtained in pure form. Patterns of **1**, **5**, and **6** were, however, found to have very weak peaks that did not match the structure determined for these phases by single crystal X-ray diffraction, suggesting the presence of trace impurity phases that could not be identified (see Figures S1−7 for Le Bail fits performed using the program Rietica[33]). High-resolution synchrotron X-ray powder diffraction patterns were obtained for both as-synthesized and exfoliated samples of **1** and **7**, held in glass capillaries, using beamline I11 at the Diamond Light Source U.K.[34,35] A wavelength of 0.827153(1) Å and the Mythen position sensitive detector were used, and the more complex peak shape of this data, caused by the peak shape being dominated by sample broadening, required the use of the program GSAS[36] for refinements. Microanalysis results for all compounds, except **6**, suggest that these have chemical compositions consistent with single crystal X-ray diffraction, which indicates that the impurities in samples of **1** and **5** are particularly small (see Table S2).

Thermogravimetric analysis (TGA) of the bulk frameworks was performed in air on a TA Instruments Q500 using a heating rate of 10 °C/min. The Mn, Co, and Zn compounds appear to fully decompose above 250, 320, and 370 °C, respectively, although hydrated phases typically begin to lose their water molecules below 130 °C (see SI for further details and Figures S8−14 for plots of the TGA data). The temperature and field dependence of the dc magnetization was

dx.doi.org/10.1021/ic302011x | *Inorg. Chem.* 2012, 51, 11198−11209

Table 2. Crystallographic Data for Structures 1−7 Determined by Single Crystal X-ray Diffraction with Structure 7 Collected from a Sample Made Using *meso*-2,3-DMS

	1	2	3	4	5	6	7
formula	$Mn_3C_{18}H_{28}O_{14}$	$MnC_6H_8O_4$	$MnC_6H_8O_4$	$Mn_2C_{12}H_{24}O_{12}$	$CoC_6H_{10}O_5$	$CoC_6H_8O_4$	$ZnC_6H_8O_4$
fw	633.22	199.06	199.06	470.19	221.07	203.05	209.49
T (K)	120(2)	125(2)	120(2)	120(2)	125(2)	120(2)	120(2)
cryst syst	monoclinic	trigonal	monoclinic	monoclinic	orthorhombic	monoclinic	triclinic
space group	$P2_1/n$ (No. 14)	$R\bar{3}$ (No. 148)	$C2/c$ (No. 15)	$P2_1/c$ (No. 14)	$Cmca$ (No. 64)	$C2/c$ (No. 15)	$P\bar{1}$ (No. 2)
a (Å)	10.0358(5)	11.2083(7)	13.4747(14)	9.8843(11)	22.682(3)	13.1799(12)	4.8543(3)
b (Å)	22.4619(10)	11.2083(7)	11.7071(13)	11.4178(14)	7.0298(3)	11.6913(8)	6.7522(5)
c (Å)	11.2067(7)	30.269(3)	4.8928(4)	15.884(2)	10.4274(6)	4.7525(3)	11.7208(6)
α (deg)	90	90	90	90	90	90	105.932(5)
β (deg)	111.178(6)	90	108.007(1)	90.785(10)	90	108.393(9)	92.578(4)
γ (deg)	90	120	90	90	90	90	95.916(5)
V (Å^3)	2355.6(2)	3293.1(4)	734.03(13)	1792.5(4)	1662.6(3)	694.90(9)	366.37(4)
Z	4	18	4	4	8	4	2
ρ_{calcd} (g cm^{-3})	1.786	1.807	1.801	1.742	1.766	1.941	1.899
μ (cm^{-1})	13.583	1.768	1.753	12.032	2.043	2.420	3.311
reflns measured/ unique	8497/4513 [R_{int} = 0.0456]	7397/2472 [R_{int} = 0.0493]	1776/848 [R_{int} = 0.0296]	4309/2547 [R_{int} = 0.0701]	2007/987 [R_{int} = 0.0320]	4491/1165 [R_{int} = 0.0367]	5164/1729 [R_{int} = 0.0248]
params refined	334	107	52	220	63	52	102
R1, wR2[a] (all)	0.0757, 0.1717	0.0561, 0.1377	0.0491, 0.1031	0.0945, 0.2329	0.0666, 0.1275	0.0547, 0.1227	0.0261, 0.0576
R1, wR2[a] (obsd)	0.0624, 0.1581	0.0509, 0.1319	0.0396, 0.0953	0.1184, 0.2514	0.0445, 0.1121	0.0468, 0.1157	0.0233, 0.0562
χ^2	1.010	1.037	1.023	1.044	1.018	1.063	1.051

[a] $w = 1/[\sigma^2(F_o^2) + (aP)^2 + bP]$ and $P = (\max(F_o^2, 0)+2F_c^2)/3$; R1 = $\sum||F_o| - |F_c||/\sum|F_o|$ and wR2 = $(\{\sum[w(F_o^2 - F_c^2)^2]/\sum w(F_o^2)^2\})^{1/2}$.

measured with a Quantum Design MPMS 5XL SQUID magnetometer. Powder samples were gently ground, contained in gel caps, and held in a straw with a uniform diamagnetic background. Experimental details and results from infrared spectroscopy are described in the SI.

Layered compounds **1**, **5**, and **7** were exfoliated in ethanol using an ultrasonication bath operating at 37 kHz (Elmasonic S30, 80 W). The setup and type of solvent adopted here were the same as those previously reported in the formation of MnDMS and ZnDMS nanosheets.[18,19] In addition, we have explored the effects of sonication time in an attempt to differentiate the ease of exfoliation of the different layered structures, including MnDMS and ZnDMS. Further details of the exfoliation studies and the characterization of the exfoliated materials by spectroscopic and atomic force microscopy (AFM) are presented in the SI.

3. RESULTS AND DISCUSSION

3.1. Structures of the Transition Metal 2,3-DMS Frameworks. *3.1.1. Structure of Compound 1, Mn_3(D,L-2,3-DMS)$_3$(H_2O)$_2$.* Compound **1**, also referred to as *M*n 2,3-DMS by analogy with the layered 2,2-DMS frameworks, features approximately 1 nm thick covalently bound layers that are capped on both sides by hydrophobic regions created by the methyl groups protruding into the interlayer areas (see Figure 1a). This is similar to the frameworks formed with the 2,2-DMS ligand, but the methyl groups in **1** are focused around central points in the interlayer regions in a way not found in the structures containing the 2,2-DMS isomer, leading to a significantly more corrugated layers.[18,19] The covalently bound layers also feature a different topology from the 2,2-DMS frameworks with zigzag chains of MnO_6 octahedra bridged in the other direction by the backbone of the dicarboxylate ligand (see Figure 1b). The structure has I^1O^1 connectivity overall, according to the terminology of Cheetham et al.[32] The asymmetric unit of **1** contains three Mn cations, three 2,3-DMS ligands, and two coordinated water molecules (see Figure S15). Two of the distinct Mn cations (Mn1 and Mn2) are contained in edge-sharing dimers, with neighboring dimers bridged by sharing corners with the $Mn3O_6$ octahedra to complete the chain. All Mn cations have bond valencies consistent with the divalent oxidation state, between 2.05 and 2.11.[37,38]

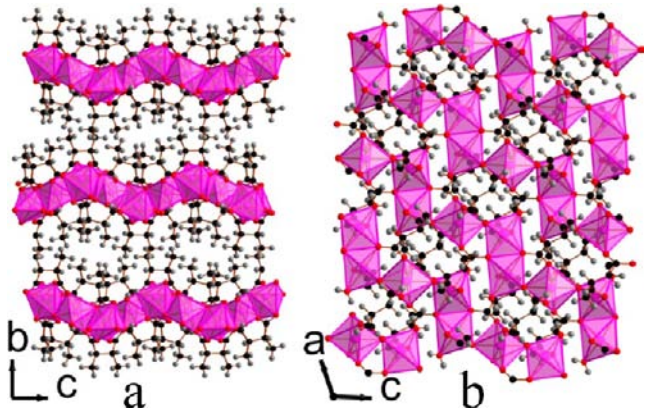

Figure 1. Structure of **1** featuring (a) the arrangement of neighboring layers and the hydrophobic region between them and (b) a depiction of a single layer in the structure. The manganese, carbon, oxygen, and hydrogen atoms are pink, black, red, and gray, respectively, and the MnO_6 octahedra are the same color as the Mn cations.

The ligands in **1** are an equal mixture of the D- and L-isomers, which are arranged such that those from the cap on the top of a layer are from one hand and those from the caps on the bottom side of the same layer and the bottom side of the layer above it feature the other hand. The oxygen atoms in the three distinct ligands all bond to at least one Mn cation, although each ligand has different overall connectivity; for example, in one ligand one oxygen atom binds to two cations while in another two oxygen atoms coordinate to two different Mn. This gives rise to (1111), (1112), and (1212) arrangements.[29,31] In all three

dx.doi.org/10.1021/ic302011x | *Inorg. Chem.* 2012, 51, 11198−11209

ligands the methyl and carboxylate groups are both close to *gauche* arrangements, compared to functional groups of the same type, although the ligand with (1111) connectivity is closer to an ideal arrangement. The coordination environments of the cations and details of the hydrogen bonding in the structure are presented in the SI, along with similar details for other structures described in this work. The torsion angles between the functional groups in all structures examined are presented in Table S3.

3.1.2. Structure of Compound **2**, *Mn(meso-2,3-DMS).* The structure of compound **2** has covalent bonding in three dimensions, unlike compound **1** and the 2,2-DMS frameworks reported to date, and the structure can be considered to have I^2O^1 connectivity overall (see Figure 2).[18,19] Compound **2** is

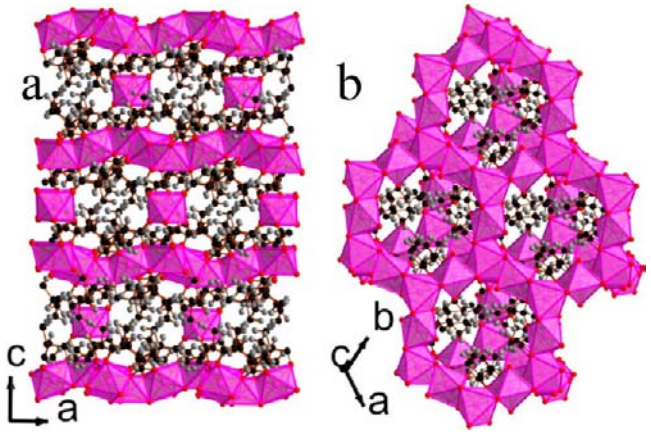

Figure 2. Structure of **2** depicting (a) the *ac* plane highlighting the arrangement of the two different types of layers and (b) the *bc* plane showing the offset between adjacent layers of rings. The colors are the same as in Figure 1.

very similar to the $Mn(C_5H_6O_4)$ framework previously synthesized by Li et al.,[39] which contains the 2-methylsuccinate ligand. Its asymmetric unit consists of three Mn cations, all of which are on special positions, and a *meso*-2,3-DMS ligand whose backbone and methyl carbons are disordered over two sites (see Figure S16). Compound **2** consists of alternating layers of 12-membered rings of edge-sharing MnO_6 octahedra and sheets containing isolated MnO_6 octahedra, with these alternating layers being bridged by the carboxylate groups. The octahedra in the latter sheets are approximately 11 Å apart and are only connected through the adjacent layers. As is the case for the Mn(2-methylsuccinate) framework, the methyl groups occupy the space between the isolated octahedra. The rings in the other layers are interconnected *via* every second MnO_6 octahedra, such that each ring is linked with six other rings in an edge-sharing fashion. The Mn cations have bond valencies between 1.80 and 2.01 and the dicarboxylate ligand, which has (1212) connectivity, has one of its methyl groups and carboxylate groups in an arrangement close to *eclipsed*.[29,31,37,38]

3.1.3. Structure of Compound **3**, *Mn(meso-2,3-DMS).* Compound **3** is another example of an architecture that can accommodate the *meso*-2,3-DMS ligand in a structure with three-dimensional covalent bonding with I^1O^2 connectivity overall. It consists of corrugated edge sharing-chains of MnO_6 octahedra, which run parallel to the *c*-axis and are bridged in the other two dimensions through the backbone of the dicarboxylate ligand (see Figure 3). The asymmetric unit of **3** consists of one Mn, which occupies a special position, and half

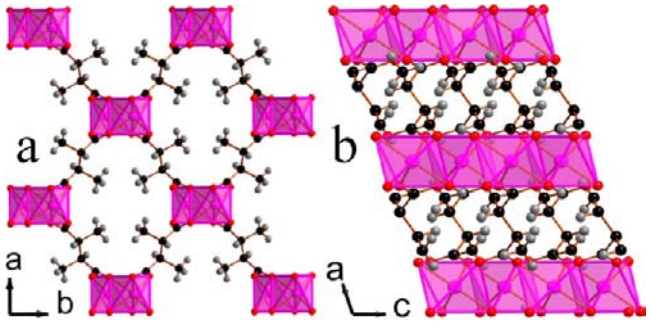

Figure 3. Structure of compound **3** depicting (a) the organic connectivity and location of the methyl groups in the structure and (b) the edge-sharing MnO_6 chains. Colors are as in Figure 1.

of a DMS ligand (see Figure S17). Looking down the *c*-axis, the chains can be viewed as being arranged into a squarelike lattice with the space inside the square primarily occupied by the methyl groups from the dicarboxylate ligands, which all adopt the *meso*-conformation. The Mn cations have a bond valency of 2.10 bonding to six different carboxylate groups.[37,38] The ligands exhibit (1212) connectivity, with their methyl and carboxylate groups arranged in a *trans*-fashion, as required by symmetry, relative to functional groups of the same type on the neighboring backbone carbon.[29,31]

3.1.4. Structure of Compound **4**, *Mn(meso-2,3-DMS)-(H_2O)·H_2O.* Similarly to **3**, the structure of **4** has I^1O^2 connectivity overall with chains of distorted MnO_6 octahedra bridged in the other two dimensions by the backbone of the carboxylate ligands (see Figure 4). The asymmetric unit of **4**

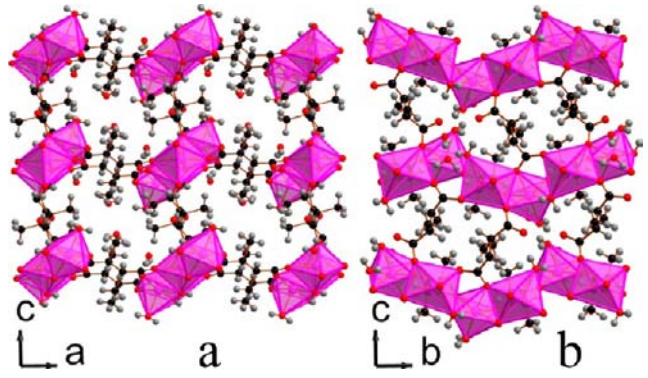

Figure 4. Structure of compound **4** showing (a) the organic connectivity and the location of the methyl groups and (b) the corrugated MnO_6 octahedral chains. The colors are as in Figure 1.

features two Mn cations, two *meso*-DMS ligands, and four water molecules (see Figure S18). The chains in **4** are more corrugated than found in **3**, and each octahedron shares an edge with one neighbor and a corner with another in the chain. While the chains do not appear to be further apart in **4** than was the case in **3**, it seems that their increased corrugation and a slight staggering of the position of adjacent DMS ligands create more space within a square notated by the position of four chains. This enables both the methyl groups and also the extra-framework water to be contained within these spaces. The other two distinct water molecules in the structure are coordinated to the Mn cations, with one of these two molecules bonding to both distinct Mn cations in the structure, providing the corner-sharing connectivity within the chains.

dx.doi.org/10.1021/ic302011x | *Inorg. Chem.* 2012, 51, 11198−11209

The two distinct Mn cations have bond valencies within 10% of 2.[37,38] Both the methyl and carboxylate functional groups on the two ligands are arranged in close to a *trans*-fashion, although the ligand with (1111) connectivity is closer to an ideal arrangement than that with (1102).[29,31]

3.1.5. Structure of Compound **5**, *Co(D,L-2,3-DMS)(H_2O).* Similar to **1** and the 2,2-DMS frameworks,[18,19] compound **5** (also known as Co 2,3-DMS) consists of 1 nm thick two-dimensionally covalently bonded layers capped with the hydrophobic methyl groups (see Figure 5a). Its asymmetric

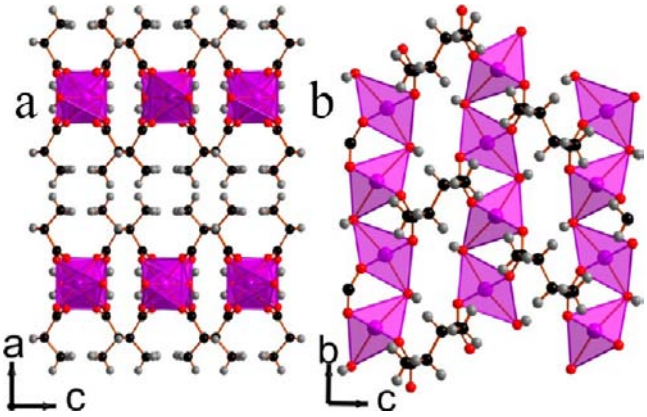

Figure 5. Structure of **5** showing (a) the arrangement of neighboring covalently bound layers and (b) the topology of one layer. The color of the Co cations and CoO_6 tetrahedra is purple, and all others are as in Figure 1.

unit consists of a Co cation, half a 2,3-dicarboxylate ligand, and an oxygen and one hydrogen from a water molecule (see Figure S19). The Mn cation and the oxygen of the water molecule are on special positions, and the dicarboxylate ligands in the structure are D- and L-, alternating along the *b*-axis. As in CoDMS, the layers feature corner-sharing chains of CoO_6 octahedra connected through the coordinated water molecules; neighboring chains are bridged by the backbone of the organic ligand, leading to the structure featuring I^1O^1 connectivity (see Figure 5b).[19] The methyl groups are arranged in the interlayer region in a similar fashion to CoDMS, although in **5** they are not disordered. The Co cations have a bond valence of 2.03, and the dicarboxylate ligands have (1111) connectivity, with their methyl and carboxylate groups arranged in a *gauche*-fashion, compared to neighboring functional groups of the same type.[29,31,37,38]

3.1.6. Structure of Compound **6**, *Co(meso-2,3-DMS).* Compound **6** is isostructural with **3**, featuring edge-sharing chains of CoO_6 octahedra bridged in the other two dimensions by the backbone of the dicarboxylate ligands (see Figures S20 and S21 for depictions of the crystal structure). The Co cations have a bond valence of 2.02, consistent with Co^{2+}, and the *meso*-2,3-dicarboxylate ligands express (1212) connectivity.[29,31,37,38] Both the carboxylate and methyl functional groups of the ligand adopt a *trans*-arrangement, as required by the symmetry of the structure.

3.1.7. Structure of Compound **7**, *Zn(D,L-2,3-DMS).* The structure of **7** (also referred to as Zn 2,3-DMS) features 1 nm thick, two-dimensionally covalently bonded layers capped by the methyl groups of the carboxylate ligands (see Figure 6a). Thus, although not all 2,3-DMS frameworks adopt structures suitable for exfoliation, such compounds do form with all three

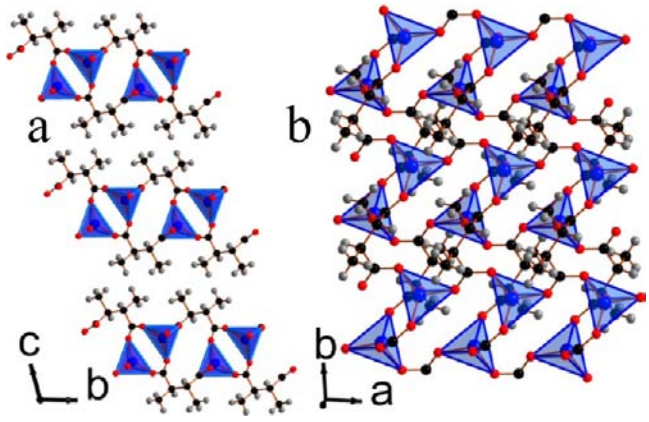

Figure 6. Structure of compound **7** showing (a) the arrangement of neighboring layers and (b) the topology of an individual layer. The zinc cations and ZnO_4 tetrahedra are blue, and all other colors are as in Figure 1.

transition metals examined in this study. The asymmetric unit of **7** features one Zn cation and a 2,3-DMS ligand (see Figure S22); the topology of its layers are significantly different than that adopted by **1** or **4**, highlighting the variation possible while retaining a structure suitable for exfoliation. The layers consist of tetrahedral Zn dimers bridged by two carboxylate groups with dimers linked, *via* one carboxylate group per Zn cation, to neighboring dimers into a row along the *a*-axis (see Figure 6b). Rows of dimers are linked *via* the backbone of the carboxylate ligands leading to the formation of an I^0O^2 structure. As was the case for the other layered structures, the dicarboxylate ligands are a 50:50 mixture of D- and L-isomers, regardless of whether the framework is synthesized from a mixture of isomers or the pure *meso*-ligand. They are arranged in a similar fashion to **1**, with the ligands on the top of a layer all being one isomer and those on the bottom of the same layer and that of the one above it having the other handedness. The Zn cations are bonded to four separated dicarboxylate ligands and have a bond valency of 2.08.[37,38] This leads the carboxylate oxygen atoms to adopt (1111) connectivity, while the carboxylate and methyl groups of the ligand adopt a *gauche*-arrangement, compared to the identical functional groups on the neighboring backbone carbon.

3.2. Phase Diversity and the Isomeric Effect on the Formation of Two- and Three-Dimensional Structures. There appears to be greater structural diversity among the Mn^{2+} frameworks reported here than is found for either the Co or Zn compounds. The hydrated phase, **1**, forms at lower temperatures when an isomeric mixture of ligand is used, while anhydrous **2**, which has I^2O^1 connectivity, forms at higher temperatures. Interestingly, phase **2** features the *meso*-2,3-DMS ligand, while **1** features a mixture of D- and L-isomers, suggesting increased temperature may favor the formation of phases containing the *meso*-ligand, as found in the case of Sr tartrate by Appelhans et al.[40] When *meso*-2,3-dimethylsuccinic acid is used in a reaction at 100 °C, structure **4** forms, which has two water molecules per Mn cation and I^1O^2 connectivity. Temperatures above this lead to the formation of **3**, which is anhydrous but still I^1O^2, while above 180 °C phases **2** and **3** form as part of a two phase mixture. Therefore, although three phases form at different temperatures when the purely *meso*-isomer of the ligand is used, the general trend of increasing dehydration and inorganic connectivity with increasing temper-

ature remains, consistent with previous studies of dicarboxylate frameworks.[19,23,25]

In contrast, only **5** forms for reactions using Co and the isomeric mixture of 2,3-dimethylsuccinic acid at all temperatures examined in this study. In reactions using the pure-*meso*-isomer, however, **6** only forms above 180 °C, with a different phase forming below this temperature for which, unfortunately, it was not possible to obtain crystals suitable for structure determination. Compound **7** is unusual compared to the other phases examined in this work as it forms in significant quantities from reaction using both the isomeric mixture and pure *meso*-isomer. This is an interesting result as its formation in the latter case requires the isomerization of the *meso*-isomer to a mixture of D- and L-isomers. A higher reaction temperature is required to form **7** when the *meso*-ligand is used, suggesting isomerization only occurs at higher temperature. This is analogous to observations from the formation of Sr and Ba tartrates.[40]

Unlike the transition metal 2,2-DMS frameworks, which ubiquitously form two-dimensional covalently bonded structures with only weak interactions between layers, only three out of the seven frameworks containing the 2,3-isomers form such structures.[18,19] There is a clear divide between the layered structures formed when the D- and L-2,3-DMS isomers are incorporated into a structure and the three-dimensional covalent connectivity that occurs in frameworks featuring the *meso*-ligand. Examination of the torsion angles in the frameworks incorporating the D- and L-ligands shows that the methyl groups are arranged in a *gauche*-fashion, which is also true for the carboxylate groups (see Figure 7). In three of the four frameworks featuring the *meso*-ligands, however, the methyl and carboxylate groups are arranged in a *trans*-fashion to the functional group of the same type on the neighboring backbone carbon atom. Some insight into this behavior can be found from the different conformers of the depronated 2,3-DMS isomers in solution. The work of Morawetz and Choi[41] showed that, in water, the *meso*-2,3-DMS ligand prefers to adopt the *trans*-arrangement found in the majority of the frameworks in this study, with this being favored by both electrostatic and steric factors. In contrast, they suggest that both electrostatic and steric factors favor the D- and L-ligands having their methyl groups *gauche* to each other, although electrostatic repulsion favors this being done in such a way that the carboxylate groups are *trans* while steric factors favor a *gauche*-arrangement. In the case of framework compounds, the bonding between the cations and ligands will be partially covalent, reducing the importance of electrostatic repulsion between the carboxylate groups, so it is unsurprising that the *gauche*-arrangement of both methyl and carboxylate groups on neighboring carbons dominates.

Figure 7. View along the central C−C bond of the arrangements of the methyl and carboxyl functional group favored by the D- and L-structures (left), the *meso*-ligands (middle), and the *eclipsed*-arrangement found in structure **2** (right).

The different arrangements of the functional groups adopted by the D- and L-structures compared with the *meso*-ligands have two principal effects. First, it places the methyl groups on the same side of the ligand in the case of the D- and L-isomers, but on opposite sides and therefore further apart, in the case of the *meso*-ligands. Additionally, it leads to the *meso*-ligand acting as a linear linker while the D- and L-ligands link in a bent fashion. The *gauche*-geometry of the methyl groups in the D- and L-ligands places them in an ideal position to be thrust out into the interlayer spacing in a layered structure with two-dimensional covalent connectivity, similar to the effect of the 2,2-DMS ligand. This effect is reinforced by the bent linkage provided by the *gauche*-arrangement of the carboxylate groups. Since, however, maleate frameworks also have carboxylate groups in a bent arrangement but form structures with covalent connectivity between one and three dimensions, this is not sufficient in isolation to strongly favor formation of a layered structure in the absence of the bulky methyl groups.[42−45] One example where the arrangement of the carboxylate groups does lead to the formation of exclusive layered structures is the 4-cyclohexene-1,2-dicarboxylate frameworks, although they adopt a *trans*-configuration, and also have a bulky element to their structure in the form of the cyclic ring.[46] In contrast, the *trans*-arrangement of the methyl groups in the *meso*-isomer reduces the steric barrier to accommodating the *meso*-ligand in a three-dimensional structure and would most likely require that the methyl groups jut out into opposite sides of a layered structure should one form. The linear bridge provided by the *meso*-isomer when the carboxylate groups are *trans* is clearly visible in three of the four structures and favors the organic bridging of structures featuring one-dimensional inorganic chains. The one exception to the *meso*-ligand adopting the *trans*-geometry described above is compound **2**; here, an *eclipsed* arrangement of one methyl group and one carboxylate group from adjacent carbon atoms is found, with the neighboring methyl groups and neighboring carboxylate groups separated by close to 120° (see Figure 7). Since this structure only forms at high temperatures it appears to be the thermodynamically favored Mn framework, with its more extensive inorganic connectivity compensating for both the sterically and electrostatically unfavorable arrangement of the ligand.

3.3. Nanosheet Exfoliation of Two-Dimensional Frameworks. The liquid exfoliation of 2,3-DMS layered compounds **1**, **5**, and **7** *via* ultrasonication is readily achievable and simple. As noted for the 2,2-DMS layered frameworks, namely MnDMS and ZnDMS,[18,19] ethanol is the preferred exfoliation agent for the DMS family due to the efficiency with which it dissociates the weakly bound 2-D layers and prevents isolated films from subsequently reassembling (see Figure 8).

The kinetics of the exfoliation process itself, however, have not been elucidated to date. To study this, we have applied an approach recently successfully implemented for characterizing nanosheet dispersions in a wide range of solvents.[20] This requires the extinction coefficients (α) of the different nanosheet suspensions to be determined by means of absorption spectroscopy, from which the concentration (C) of the exfoliated material can then be determined through the Beer−Lambert law (i.e., $A/L = C\alpha$, where A/L is the absorbance per unit length). To illustrate this, Figure 9a presents the absorption spectra of the *M*n 2,3-DMS (**1**) suspension with concentrations varying from 0.1 to 0.02 mg/mL; similar spectra were obtained for compounds **5**, **7**, MnDMS, and ZnDMS, albeit with relatively lower intensities

dx.doi.org/10.1021/ic302011x | *Inorg. Chem.* 2012, 51, 11198−11209

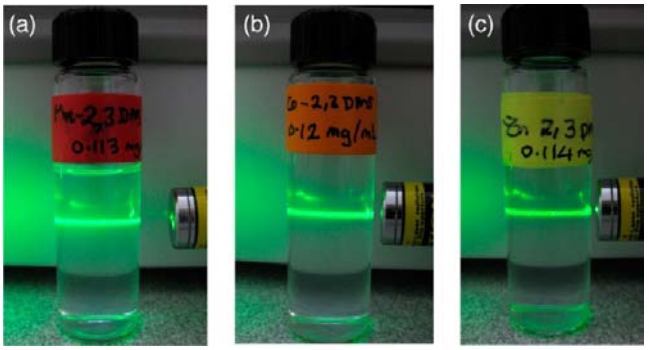

Figure 8. Demonstration of the Tyndall effect in colloidal suspensions comprising nanosheets of (a) *M*n 2,3-DMS **1**, (b) Co 2,3-DMS **5**, and (c) Zn 2,3-DMS **7** in an ethanol solvent, all of which had been ultrasonicated for 1 h. The nominal concentration of the supernatant was ∼0.1 mg/mL.

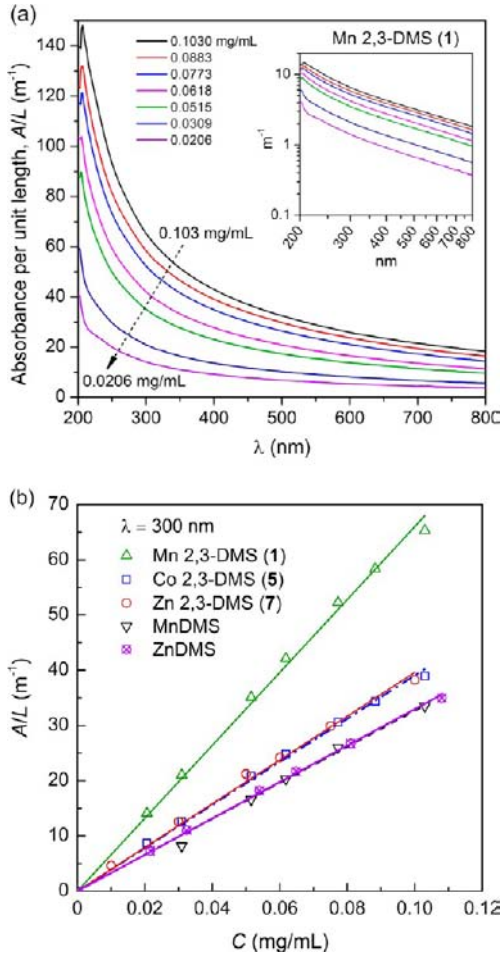

Figure 9. (a) Absorption spectra of nanosheet suspensions of *M*n 2,3-DMS (**1**) at different concentrations; the inset shows the data on a log−log scale with the linear correlation at higher wavelengths indicative of light scattering contributing strongly to the observed behavior. The spectra obtained from compounds **5**, **7**, MnDMS, and ZnDMS appear in Figure S23 in the SI. (b) Beer−Lambert plots at a defined wavelength of 300 nm, in which the extinction coefficients (gradient $\alpha = (A/L)/C$) of **1**, **5**, **7**, MnDMS, and ZnDMS have been found to be 660.2, 373.8, 396.1, 326.2, and 329.7 mL mg^{-1} m^{-1}, respectively.

(see Figure S23). Characteristic d−d transitions in Mn and Co were not observed, probably due to the dilute nature of the dispersions employed, and may suggest that light scattering contributes strongly to the observed behavior. Consequently, a fixed wavelength at 300 nm was defined for calculating the extinction coefficients based on the Beer−Lambert plots in Figure 9b, where the corresponding values of A/L and C are linearly correlated.

Importantly, the above information allows us to establish the concentration as a function of sonication time for the different compounds, the results of which are summarized in Figure 10.

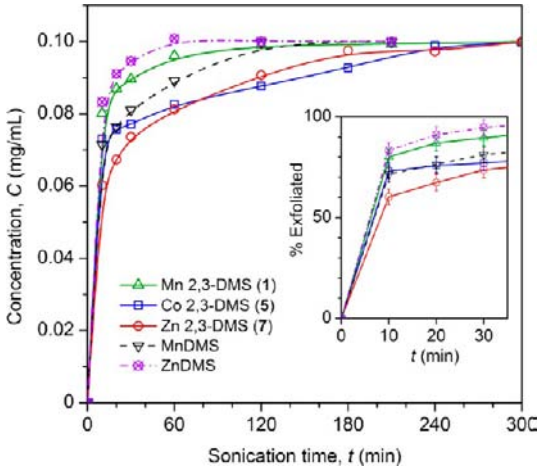

Figure 10. Exfoliation kinetics of 2,3-DMS and 2,2-DMS layered frameworks, in which the maximum concentration was 0.1 mg/mL (inset, equivalent to 100%). Figure S24 in the SI presents the corresponding absorbance spectra measured at varying sonication times, from which the concentrations were determined according to $C = (A/L)/\alpha$.

While the ease of exfoliation of the layered frameworks appears to be distinct for each system, it is clear that a relatively short sonication time of about 20 min is adequate to achieve a high degree of exfoliation (above 70% as in Figure 10 inset); this system is thus ideal for high-throughput nanosheets production. Interestingly, our findings indicate that *M*n 2,3-DMS (**1**) and ZnDMS frameworks are the easiest to exfoliate, both exceeding 90% in 20 min (Figure 10 inset); we hypothesize that their significantly more corrugated layered architecture may help minimize the energy required for delamination.

The morphologies and the surface topographies of the finely dispersed nanosheets were characterized by atomic force microscopy (AFM). In general, we found that the exfoliated materials of **1**, **5**, and **7** constitute both fully exfoliated and partially exfoliated nanosheets (Figures 11−13), which are reminiscent of the 2,2-DMS layered frameworks.[18,19] While multilayer films exhibit relatively larger lateral dimensions, some of which are up to 10 × 10 μm^2, their thicknesses are typically greater than 100 nm. In comparison, thinner nanosheets consisting of only a few host layers (<5 nm thickness) have appreciably smaller lateral dimensions (50−100 nm "platelets") and remain dispersed in the supernatant liquid due to Brownian motion for a prolonged period of time, up to several weeks. The differences between the morphologies of the different compounds are subtle. There is, however, evidence that the exfoliation of the Co 2,3-DMS (**5**) framework yields more extended unilamellar nanosheets (∼1 nm thickness) with lateral sizes of ∼500 nm; some representative examples are

dx.doi.org/10.1021/ic302011x | *Inorg. Chem.* 2012, 51, 11198−11209

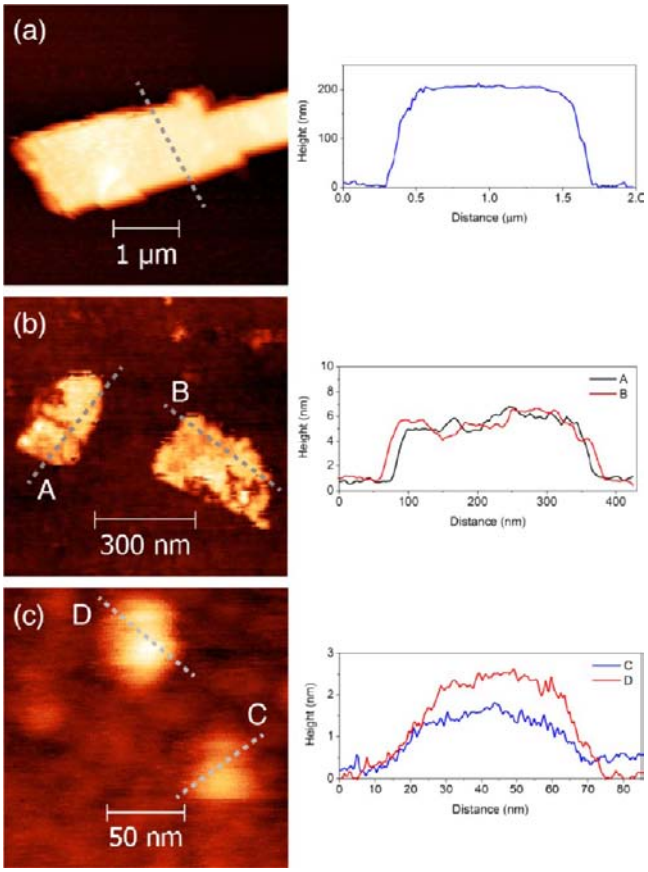

Figure 11. AFM height topography and cross-sectional profiles of *M*n 2,3-DMS (**1**) nanosheets sonicated for a total of 5 h. (a) A multilayer film comprising 200 host layers and of lateral dimensions of about 3 × 1 μm^2. (b) and (c) Thin nanosheets made up of 1 to 5 host layers. Additional AFM images of **1** are given in Figure S25.

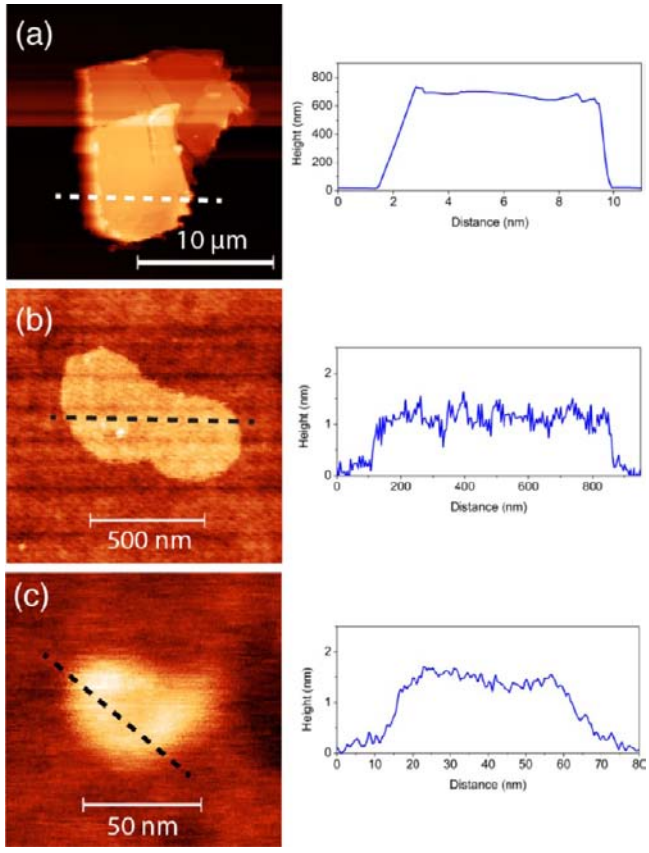

Figure 12. AFM height topography of Co 2,3-DMS (**5**) nanosheets. (a) Larger multilayer film with lateral dimensions of about 10 × 10 μm^2. (b and c) Representative unilamellar nanosheets with lateral dimensions ranging from ∼50 nm to ∼500 nm, both of which were obtained from the supernatant liquid. Additional AFM images of **5** are given in Figure S26.

shown in Figure 12b and Figure S26a,b. Here we propose that its less corrugated layered structure (Figure 5a) might have facilitated the cleaving of more extended 2-D sheets. Powder diffraction patterns were obtained of nanosheets of phases **1**, **5**, and **7**, recovered *via* centrifugation, which confirmed that the reconstituted materials adopt the same crystal structure as the bulk phase, and additionally, the lattice parameters refined from the synchrotron X-ray diffraction patterns of the reconstituted and as-synthesized samples of **1** and **7** were nearly identical (less than 0.2% difference in all cases, see Figures S28 and S29). This result suggests that there is negligible change in the crystal structure of these materials upon exfoliation. As expected, the peak shapes of the synchrotron diffraction patterns of the reconstituted samples are broader than in the as-synthesized phases, and the nature of this broadening suggests it is primarily caused by increased strain in the reconstituted samples.

3.4. Magnetic Properties of the Transition Metal 2,3-DMS Frameworks. As can be seen from Table 3, among the paramagnetic 2,3-DMS frameworks only compounds **3**, **4**, and **6** order magnetically. Compound **2** and both paramagnetic D,L-2,3-DMS frameworks, **1** and **5**, feature short-range antiferromagnetic interactions but do not exhibit any long-range order (see Figure S30). That none of the layered frameworks exhibit any long-range magnetic order is quite different from the 2,2-DMS compounds, two of which have been shown to exhibit low dimensional magnetic order.[19] This highlights the important role that the precise architecture of the layers plays in the physical properties of these compounds.

The magnetic susceptibility of **3** has a broad hump centered around 50 K (see Figure 14), consistent with low dimensional antiferromagnetic order, probably within the edge-sharing MnO_6 chains. Around 39 K, field cooled (FC) and zero-field cooled (ZFC) 0.1 kOe measurements increase significantly and diverge, but this feature is suppressed in 20 kOe measurements. This suggests that it is caused by the presence of a trace amount of a magnetic impurity, most likely Mn_3O_4 given the ordering temperature. Since there was no other indication of any impurity, the amount present must be very small. $\chi_m T$ decreases gradually from 2.9 $cm^3\ mol^{-1}$ at 300 K to nearly zero at 2 K, consistent with antiferromagnetic behavior (see Figure 14 insert). Well above its magnetic ordering temperature, **3** is a Curie−Weiss paramagnet, with a Θ value of −178 K, consistent with predominantly antiferromagnetic interactions, and a μ_{eff} of 6.09 μ_B, close to the spin-only moment of 5.92 μ_B expected for high spin Mn^{2+}. A plot of $C/(\chi|\Theta|) - 1$ as a function of $T/|\Theta|$ (where C = the Curie constant and χ = the magnetic susceptibility) reveals a positive deviation from Curie−Weiss behavior near the Curie−Weiss temperature, consistent with purely antiferromagnetic behavior (see Figure S31).[47]

Magnetic susceptibility measurements of **4** peak at around 7 K, indicating the onset of antiferromagnetic order (see Figure 15). This feature is much sharper than that found in **3** and is consistent with **4** exhibiting three-dimensional magnetic order.

dx.doi.org/10.1021/ic302011x | *Inorg. Chem.* 2012, 51, 11198−11209

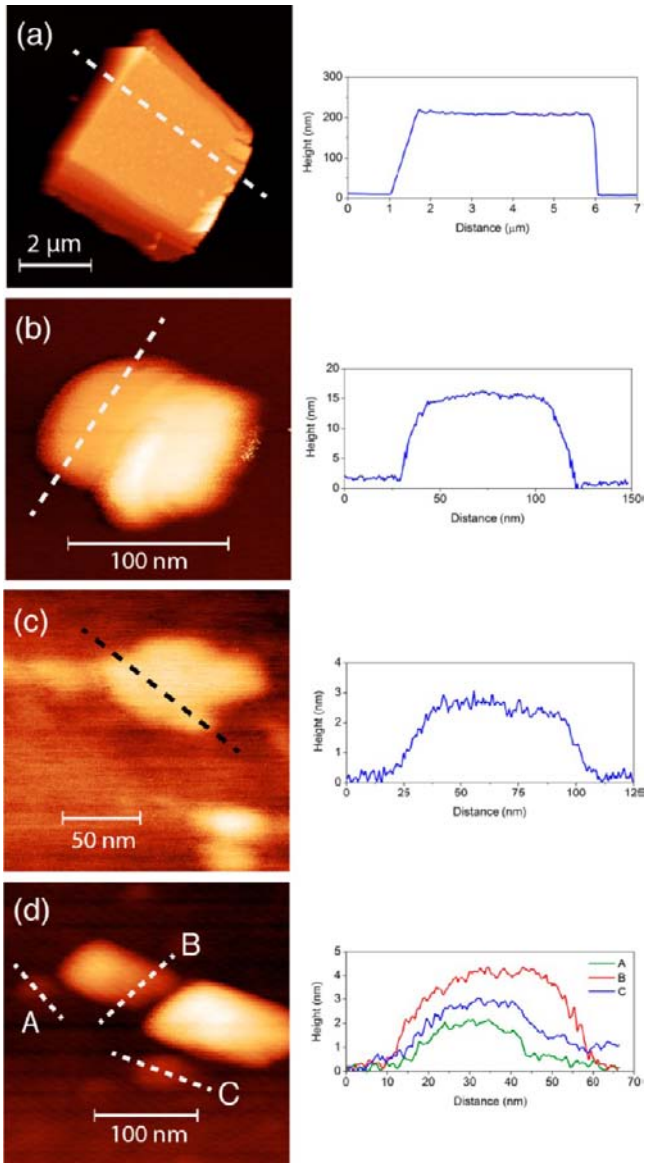

Figure 13. AFM height topography of Zn 2,3-DMS (**7**) nanosheets. (a) Multilayer film with a thickness of ~200 nm and lateral dimensions of 3 × 3 μm^2. (b) Thin film comprising 15 host layers and with a lateral dimension of 100 × 100 nm^2. Parts c and d illustrate the typical morphologies of nanosheet dispersions (sampled from supernatant) with thicknesses of just a few nanometers and featuring a lateral dimension of up to 100 nm. Additional AFM images of **7** are shown in Figure S27.

Table 3. Magnetic Behavior of the Paramagnetic 2,3-DMS Frameworks[a]

compd	connectivity	long range magnetic behavior	ordering temp (K)	Θ (K)	μ_{eff} (μ_B)
1	2D (I^1O^1)	paramagnet	N/A	−13.4	5.92
2	3D (I^2O^1)	paramagnet	N/A	−13.1	5.74
3	3D (I^1O^2)	1D antiferromagnet	50	−178	6.09
4	3D (I^1O^2)	3D antiferromagnet	7	−10.4	5.84
5	2D (I^1O^1)	paramagnet	N/A	−17.2	5.13
6	3D (I^1O^2)	3D antiferromagnet	6	18.3	4.58

[a]Curie−Weiss fits have been performed on 0.1 kOe zero-field cooled data, and Θ is the Curie−Weiss Θ.

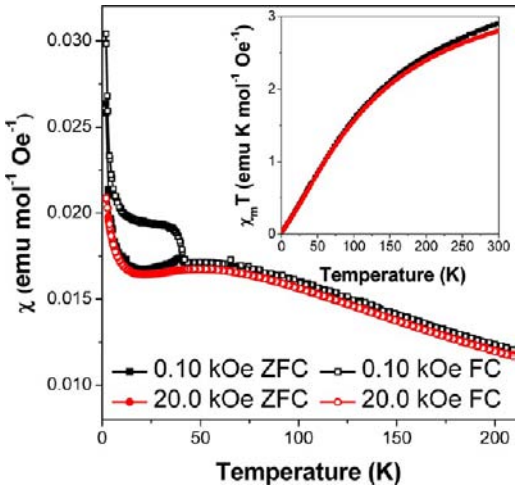

Figure 14. Magnetic susceptibility of **3** versus temperature. The insert shows the behavior of $\chi_m T$ with temperature.

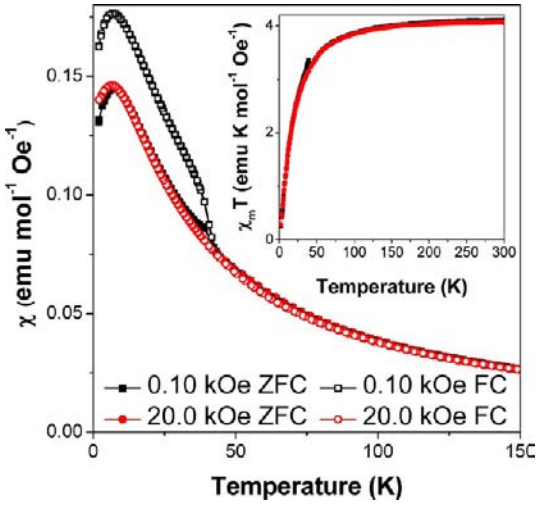

Figure 15. Magnetic susceptibility of **4** versus temperature. The insert shows the behavior of $\chi_m T$ with temperature.

As expected in the presence of predominantly antiferromagnetic interactions, $\chi_m T$ decreases from 4.1 cm^3 mol^{-1} at room temperature to near zero at 2 K, with the sharpest decrease occurring below 50 K (see Figure 15 insert). Above the ordering temperature, compound **4** is a Curie−Weiss paramagnet, with a Θ of −10.4 K and a μ_{eff} of 5.84 μ_B, close to the value expected for high spin Mn^{2+}. A plot of inverse scaled magnetic susceptibility versus scaled temperature deviates positively from Curie−Weiss behavior well above Θ, suggesting that purely antiferromagnetic interactions occur well above the ordering temperature (see Figure S31). The Mn−O−Mn bond angles in this compound are approximately 100−110°, a range in which the Goodenough−Kanamori rules suggest the intrachain interactions could be either antiferromagnetic or ferromagnetic.[48,49] It would therefore be necessary to determine the magnetic structure of this compound using neutron diffraction to fully understand its magnetic behavior.[28,50−52] Similarly to compound **3**, the magnetic susceptibility of **4** in low applied fields exhibits features around 39 K. They are suppressed in higher applied fields, which suggest the presence of a trace amount of Mn_3O_4 that was not evident in other analyses.

dx.doi.org/10.1021/ic302011x | Inorg. Chem. 2012, 51, 11198−11209

FC susceptibility measurements of **6**, in 0.02 and 0.1 kOe fields, exhibit a peak around 6 K suggesting the onset of antiferromagnetic order (see Figure 16). Increasing the applied

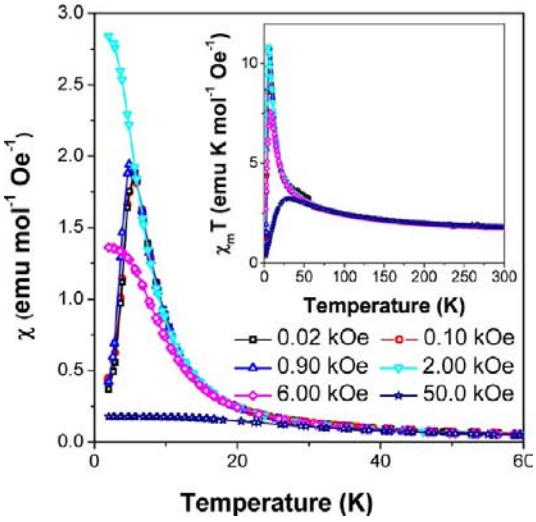

Figure 16. Field cooled magnetic susceptibility of compound **6** versus temperature. The insert shows the behavior of $\chi_m T$ with temperature.

field to 0.9 kOe, however, appears to suppress the ordering temperature slightly, and in higher applied fields the susceptibility continues to increase below 6 K. $\chi_m T$ increases with decreasing temperature in all applied fields examined, suggesting that there is a strong ferromagnetic-like component to the interactions in **6**. $\chi_m T$ peaks near 6 K, for all the measurements conducted in fields below 6 kOe, consistent with the onset of long-range magnetic order around this temperature (see Figure 16 insert). Above the ordering temperature, **6** is a Curie–Weiss paramagnet with a Θ of 18.3 and a μ_{eff} of 4.58 μ_B, within the range 3.88–5.20 μ_B expected for Co^{2+} cations. A plot of $C/(\chi|\Theta|) + 1$ as a function of $T/|\Theta|$, from a 0.1 kOe measurement, however, deviates positively from Curie–Weiss behavior above Θ. This suggests that the short-range antiferromagnetic interactions in **6** are significant well above the Θ despite clear indications, from the Curie–Weiss fit, that the nearest neighboring interactions are ferromagnetic (see Figure S31).

An isothermal magnetization measurement at 1.9 K suggests that *M* increases slowly below 1 kOe but rises rapidly above this (see Figure 17). There is an inflection point in d*M*/d*H* at 1.4 kOe indicative of a magnetic phase transition, consistent with the magnetic susceptibility measurements in higher fields (see Figure 17 insert). The magnetization value is close to saturated in a 10 kOe field at 2.47 μ_B mol^{-1} and only slowly increases after that to 2.61 μ_B mol^{-1} at 50 kOe. The observed saturation is consistent with a transition to a ferrimagnetic or ferromagnetic phase above 1.4 kOe, and since the structure has only one unique Co site, it is most likely to be ferromagnetic.

The observation that the dominant interactions in **6** appear to be ferromagnetic but the ordered state in low fields is antiferromagnetic suggests that the magnetic moments of the Co within a CoO_6 chain are probably ferromagnetically coupled while neighboring chains interact antiferromagnetically. Our interpretation is consistent with the intrachain Co–O–Co bond angle, which at 86.00(7)° is very close to 90°, from which ferromagnetic coupling would be expected for a high spin d^7

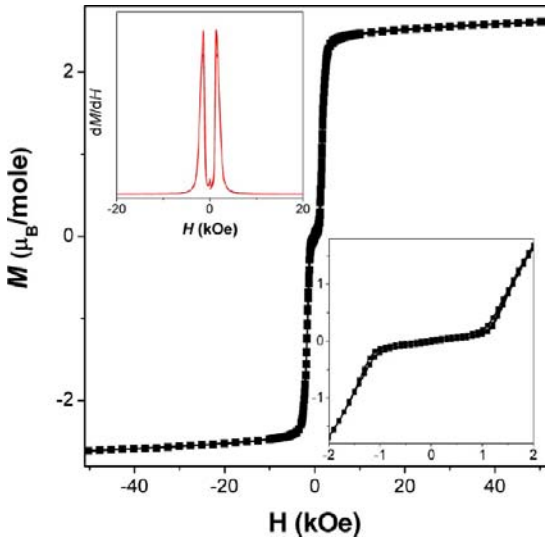

Figure 17. Isothermal magnetization measurement of **6** at 1.9 K. The inserts show the derivative of the magnetization, highlighting the transition at 1.4 kOe (top left), and a closer view of the low field section of the measurement (bottom right).

cation (see Figure S21 for intrachain Co–O–Co connectivity). This is in contrast to the behavior observed for **3**, which is isostructural and has MnO_6 octahedral chains that appear to be antiferromagnetically coupled, despite a similar Mn–O–Mn bond angle, 86.98(7)° (see Figure S17 for intrachain Mn–O–Mn connectivity). This difference is, however, consistent with the Goodenough–Kanamori rules, which predict that a superexchange angle close to 90° will lead to a ferromagnetic exchange in the case of the d^7 Co cation but either antiferromagnetic or ferromagnetic coupling in the case of d^5 Mn^{2+}.[48,49] In both compounds the interchain coupling is apparently very weak, as evidenced by **3** only exhibiting one-dimensional magnetic order and **6** requiring only a very weak applied field to cause a transition from an antiferromagnet to a ferromagnet. Antiferromagnetic–ferromagnetic transitions have been observed before in framework materials, including two which feature inorganically connected chains of Co cations, but generally at significantly higher applied magnetic fields.[53−55] It is also interesting that of the 2,3-DMS frameworks only those containing the *meso*-ligand with both types of functional groups in *trans*-positions exhibit long-range magnetic order.

4. CONCLUSION

This work reports the structures of seven transition metal 2,3-DMS frameworks. It was found that structures with two-dimensional, covalently bonded layers and weak van der Waals interlayer interactions can be made with all three cations examined in this study (Mn, Co, and Zn), but only with the D and L ligands. Those frameworks featuring the *meso*-isomer of the 2,3-DMS ligand form structures with three-dimensional covalent connectivity. This difference appears to be caused by the *meso*-isomer preferring a conformation in which its neighboring functional groups of the same type *trans* to each other, while the D- and L-ligands ubiquitously adopt *gauche*-arrangements. Thus, those frameworks incorporating the D- and L-ligands, in which the methyl groups are on the same side of the carbon backbone, adopt layered structures akin to those found in the 2,2-DMS compounds, which has a similar arrangement of methyl groups. In frameworks incorporating

dx.doi.org/10.1021/ic302011x | *Inorg. Chem.* 2012, 51, 11198–11209

the *meso*-ligand the methyl groups are significantly further apart, favoring three-dimensional structures.

The D,L-2,3-DMS ligand is shown to be suitable for designing exfoliable layered frameworks. Their ease of nanosheet exfoliation, *via* ultrasonication, has been examined using UV–vis spectroscopy and compared to those containing the 2,2-DMS ligand. It is clear that those frameworks that feature more corrugated frameworks separate more readily and rapidly, and the sizes, morphologies, and structures of the exfoliated nanosheets have been characterized using AFM and synchrotron X-ray diffraction. The magnetic properties of the six paramagnetic compounds have also been described. Only those three-dimensional frameworks containing the *meso*-2,3-DMS ligands arranged in *trans*-positions are found to order magnetically. The Mn compounds **3** and **4** order in one and three dimensions, respectively, while the Co containing framework **6**, which is isostructural to **3**, exhibits three-dimensional antiferromagnetic order in low fields and undergoes a transition to a ferromagnetic phase in slightly elevated applied fields. All layered frameworks, and the one *meso*-2,3-DMS framework where the ligand adopts an *eclipsed*-arrangement, retain paramagnetic behavior across all temperatures examined.

■ ASSOCIATED CONTENT

Supporting Information

Additional details and figures. CIF data. This material is available free of charge via the Internet at http://pubs.acs.org.

■ AUTHOR INFORMATION

Corresponding Author

*E-mail: akc30@cam.ac.uk. Fax: +44 1223 334567. Phone: +44 1223 767061.

Notes

The authors declare no competing financial interest.

■ ACKNOWLEDGMENTS

The authors would like to thank the European Research Council for financial support and acknowledge the use of MRL Central Facilities which are supported by the MRSEC Program of the NSF under Award No. DMR 1121053 (a member of the NSF-funded Materials Research Facilities Network (www.mrfn.org)). PTB is funded by the NSF Graduate Research Fellowship Program. We would also like to thank the Diamond Light Source for access to Beamline I11, which contributed to the results presented here, and Alistair Lennie and Stephen Thompson for their assistance in the use of the beamline.

■ REFERENCES

(1) Tan, J. C.; Cheetham, A. K. *Chem. Soc. Rev.* **2011**, *40*, 1059.
(2) Cheetham, A. K.; Rao, C. N. R. *Science* **2007**, *318*, 58.
(3) Férey, G. *Chem. Soc. Rev.* **2008**, *37*, 191.
(4) Fletcher, A. J.; Thomas, K. M.; Rosseinsky, M. J. *J. Solid State Chem.* **2005**, *178*, 2491.
(5) Long, J. R.; Yaghi, O. M. *Chem. Soc. Rev.* **2009**, *38*, 1213.
(6) Lee, J.; Farha, O. K.; Roberts, J.; Scheidt, K. A.; Nguyen, S. T.; Hupp, J. T. *Chem. Soc. Rev.* **2009**, *38*, 1450.
(7) Murray, L. J.; Dincă, M.; Long, J. R. *Chem. Soc. Rev.* **2009**, *38*, 1294.
(8) Jain, P.; Ramachandran, V.; Clark, R. J.; Zhou, H. D.; Toby, B. H.; Dalal, N. S.; Kroto, H. W.; Cheetham, A. K. *J. Am. Chem. Soc.* **2009**, *131*, 13625.
(9) Kurmoo, M. *Chem. Soc. Rev.* **2009**, *38*, 1353.
(10) Rao, C. N. R.; Cheetham, A. K.; Thirumurugan, A. *J Phys.: Condens. Matter* **2008**, *20*, 083202.
(11) Jacobs, B. W.; Houk, R. J. T.; Anstey, M. R.; House, S. D.; Robertson, I. M.; Talin, A. A.; Allendorf, M. D. *Chem. Sci.* **2011**, *2*, 411.
(12) Lin, W.; Rieter, W. J.; Taylor, K. M. L. *Angew. Chem., Int. Ed.* **2009**, *48*, 650.
(13) Qiu, L.-G.; Li, Z.-Q.; Wu, Y.; Wang, W.; Xu, T.; Jiang, X. *Chem. Commun.* **2008**, 3642.
(14) Spokoyny, A. M.; Kim, D.; Sumrein, A.; Mirkin, C. A. *Chem. Soc. Rev.* **2009**, *38*, 1218.
(15) Zhang, X.; Ballem, M. A.; Hu, Z.-J.; Bergman, P.; Uvdal, K. *Angew. Chem., Int. Ed.* **2011**, *50*, 5729.
(16) Amo-Ochoa, P.; Welte, L.; Gonzalez-Prieto, R.; Sanz Miguel, P. J.; Gomez-Garcia, C. J.; Mateo-Marti, E.; Delgado, S.; Gomez-Herrero, J.; Zamora, F. *Chem. Commun.* **2010**, *46*, 3262.
(17) Li, P.-Z.; Maeda, Y.; Xu, Q. *Chem. Commun.* **2011**, *47*, 8436.
(18) Tan, J.-C.; Saines, P. J.; Bithell, E. G.; Cheetham, A. K. *ACS Nano* **2012**, *6*, 615.
(19) Saines, P. J.; Tan, J.-C.; Yeung, H. H.-M.; Barton, P. T.; Cheetham, A. K. *Dalton Trans.* **2012**, *41*, 8585.
(20) Coleman, J. N.; Lotya, M.; O'Neill, A.; Bergin, S. D.; King, P. J.; Khan, U.; Young, K.; Gaucher, A.; De, S.; Smith, R. J.; Shvets, I. V.; Arora, S. K.; Stanton, G.; Kim, H.-Y.; Lee, K.; Kim, G. T.; Duesberg, G. S.; Hallam, T.; Boland, J. J.; Wang, J. J.; Donegan, J. F.; Grunlan, J. C.; Moriarty, G.; Shmeliov, A.; Nicholls, R. J.; Perkins, J. M.; Grieveson, E. M.; Theuwissen, K.; McComb, D. W.; Nellist, P. D.; Nicolosi, V. *Science* **2011**, *331*, 568.
(21) Late, D. J.; Liu, B.; Matte, H. S. S. R.; Rao, C. N. R.; Dravid, V. P. *Adv. Funct. Mater.* **2012**, *22*, 1894.
(22) Rao, C. N. R.; Matte, H. S. S. R.; Subrahmanyam, K. S.; Maitra, U. *Chem. Sci* **2012**, *3*, 45.
(23) Forster, P. M.; Burbank, A. R.; Livage, C.; Férey, G.; Cheetham, A. K. *Chem. Commun.* **2004**, *2004*, 368.
(24) Forster, P. M.; Cheetham, A. K. *Angew. Chem., Int. Ed.* **2002**, *41*, 457.
(25) Forster, P. M.; Stock, N.; Cheetham, A. K. *Angew. Chem., Int. Ed.* **2005**, *44*, 7608.
(26) Guillou, N.; Livage, C.; van Beek, W.; Noguès, M.; Férey, G. *Angew. Chem., Int. Ed.* **2003**, *42*, 643.
(27) Livage, C.; Forster, P. M.; Guillou, N.; Tafoya, M. M.; Cheetham, A. K.; Férey, G. *Angew. Chem., Int. Ed.* **2007**, *46*, 5877.
(28) Saines, P. J.; Hester, J. R.; Cheetham, A. K. *Phys. Rev. B* **2010**, *82*, 144435.
(29) Saines, P. J.; Jain, P.; Cheetham, A. K. *Chem. Sci.* **2011**, *2*, 1929.
(30) Saines, P. J.; Melot, B. C.; Seshadri, R.; Cheetham, A. K. *Chem.—Eur. J.* **2010**, *16*, 7579.
(31) Saines, P. J.; Barton, P. T.; Jain, P.; Cheetham, A. K. *CrystEngComm* **2012**, *14*, 2711.
(32) Cheetham, A. K.; Rao, C. N. R.; Feller, R. K. *Chem. Commun.* **2006**, *2006*, 4780.
(33) Hunter, B. A.; Howard, C. J. *A Computer Program for Rietveld Analysis of X-ray and Neutron Powder Diffraction Patterns*; Lucas Heights Laboratories: Sutherland, Australia, 1998.
(34) Tang, C. C.; Thompson, S. P.; Hill, T. P.; Wilkin, G. R.; Wagner, U. H. *Z. Kristallogr. Suppl.* **2007**, *26*, 153.
(35) Thompson, S. P.; Parker, J. E.; Potter, J.; Hill, T. P.; Birt, A.; Cobb, T. M.; Yuan, F.; Tang, C. C. *Rev. Sci. Instrum.* **2009**, *80*, 075107.
(36) Larson, A. C.; Von Dreele, R. B. *General Strucuture Analysis System (GSAS)*; Los Alamos National Laboratory: Los Alamos, NM, 1994.
(37) Brese, N. E.; O'Keeffe, M. *Acta Crystallogr.* **1991**, *B47*, 192.
(38) Brown, I. D.; Altermatt, D. *Acta Crystallogr.* **1985**, *B41*, 244.
(39) Li, W.; Barton, P. T.; Kiran, M. S. R. N.; Burwood, R. P.; Ramamurty, U.; Cheetham, A. K. *Chem.—Eur. J.* **2011**, *17*, 12429.
(40) Appelhans, L. N.; Kosa, M.; Radha, A. V.; Simoncic, P.; Navrotsky, A.; Parrinello, M.; Cheetham, A. K. *J. Am. Chem. Soci.* **2009**, *131*, 15375.
(41) Morawetz, H.; Choi, L.-S. *J. Phys. Chem.* **1986**, *90*, 4119.
(42) Lis, T. *Acta Crystallogr.* **1983**, *C39*, 39.

(43) Pajtasova, M.; Jona, E.; Koman, M.; Ondrusova, D. *Pol. J. Chem.* **2001**, *75*, 1209.
(44) Cernak, J.; Chomic, J.; Kappenstein, C.; Robert, F. *J. Chem. Soc., Dalton Trans.* **1997**, 2981.
(45) Zheng, Y.-Q.; Kong, Z.-P. *J. Coord. Chem.* **2003**, *56*, 967.
(46) Kim, D. S.; Forster, P. M.; de Delgado, G. D.; Park, S.-E.; Cheetham, A. K. *Dalton Trans.* **2004**, 3365.
(47) Melot, B. C.; Drewes, J. E.; Seshadri, R.; Stoudenmire, E. M.; Ramirez, A. P. *J. Phys.: Condens. Matter* **2009**, *21*, 216007.
(48) Kanamori, J. *J. Phys. Chem. Solids* **1959**, *10*, 87.
(49) Goodenough, J. B. *Magnetism and the Chemical Bond*; Interscience Publishers: New York, 1963; Vol. *1*.
(50) Mole, R. A.; Stride, J. A.; Henry, P. F.; Hoelzel, M.; Senyshyn, A.; Alberola, A.; Gómez Garcia, C. J.; Raithby, P. R.; Wood, P. T. *Inorg. Chem.* **2011**, *50*, 2246.
(51) Mole, R. A.; Stride, J. A.; Wills, A. S.; Wood, P. T. *Physica B* **2006**, *385*−*386*, 435.
(52) Saines, P. J.; Yeung, H. H. M.; Hester, J. R.; Lennie, A. R.; Cheetham, A. K. *Dalton Trans.* **2011**, *40*, 6401.
(53) Hulvey, Z.; Melot, B. C.; Cheetham, A. K. *Inorg. Chem.* **2010**, *49*, 4594.
(54) Yu, Q.; Zeng, Y.-F.; Zhao, J.-P.; Yang, Q.; Hu, B.-W.; Chang, Z.; Bu, X.-H. *Inorg. Chem.* **2010**, *49*, 4301.
(55) Jia, H.-P.; Li, W.; Ju, Z.-F.; Zhang, J. *Eur. J. Inorg. Chem.* **2006**, *2006*, 4264.